Video Individual Counting and Tracking from Moving Drones: A Benchmark and Methods

Yaowu Fan, Jia Wan, Tao Han, Andy J. Ma, Wanli Ouyang, and Antoni B. Chan

arXiv:2601.12500v2 [cs.CV] 28 May 2026

***Abstract*—Counting and tracking dense crowds in large-scale scenes is a highly practical yet challenging problem. Existing methods mostly rely on fixed-camera datasets with limited scene coverage, making them inadequate for crowd analysis in large-scale scenes. To bridge this gap, we introduce MovingDroneCrowd++, the largest video-level dataset dedicated to dense crowd counting and tracking with fast-moving drones, captured under diverse flight altitudes, camera angles, and illumination conditions. Existing methods, however, still fail to achieve satisfactory video individual counting or tracking performance under these challenging aerial conditions. To this end, we propose GD^{3}A (Global Density map Decomposition via group-wise Descriptor Association), a video individual counting method that first establishes pixel-level correspondences between pedestrian descriptors across frames via optimal transport with an adaptive dustbin score. Then, a group-wise association is adopted to guide the decomposition of global density map into shared, inflow, and outflow density maps. We further introduce a pedestrian tracking method, DVTrack (Descriptor Voting Track), which converts descriptor-level matching into instance-level association through descriptor voting. Our methods rely on the association results of group-wise multiple descriptors for each pedestrian rather than a single vector. Since intra-group matching errors do not affect the final counting and tracking results, our methods are more robust in dense crowds and challenging aerial conditions. Experiments show that our methods achieve substantial gains in both crowd counting and tracking on moving-drone videos with dense crowds and complex motions, reducing counting error by 47.4% and improving tracking accuracy by 64.6%. Code, dataset, and pretrained models are available.**

***Index Terms*—Moving Drone, Dense Crowd Analysis, Video-level Crowd Counting, Pedestrian Tracking.**

I. Introduction

In recent years, with the rapid advancement of artificial intelligence, the low-altitude economy has experienced explosive growth as an emerging industry [1]. UAVs (commonly referred to as drones) play a central role due to their mobility and flexibility [2]. By integrating drones with crowd analysis algorithms, such as counting or tracking [3]–[7], it becomes possible to perform flexible monitoring and density estimation of pedestrians in large-scale scenes, which effectively prevents crowd congestion and stampede-related accidents, and is of great significance for public safety [8].

However, existing crowd analysis algorithms and datasets mainly focus on static images captured by handheld cameras [9]–[13], or on videos recorded by fixed surveillance cameras [14]–[18] and hovering drones [19], [20] (see Fig. 1 (a) ∼ (c)). Due to the limited mobility of the capturing devices, these data can only cover crowds within fixed areas, making them unsuitable for counting or tracking dense crowds in large-scale scenes. In contrast, videos captured by moving drones enable both video individual counting (VIC) and tracking over large-scale scenes, where VIC aims to estimate the number of unique pedestrians appearing throughout an entire video. Although several related datasets, such as UAVVIC [21] and VisDrone [22], have been proposed, they suffer from several significant limitations. Most videos in UAVVIC are still captured by hovering drones with limited fields of view, and neither dataset focuses on dense crowds, with dense crowds in VisDrone even labeled as ignore regions. Moreover, their videos are mainly recorded in suburban areas with sparse crowds and limited diversity in flight altitude, viewing angle, and illumination, leading to a large domain gap from real-world dense crowd scenarios. As a result, no existing dataset simultaneously satisfies all these requirements: **dense crowds, diverse and complex environments, highly mobile drone-based acquisition, and large-scale scene coverage**.

Beyond dataset limitations, accurately counting or tracking dense crowds in videos captured by highly dynamic drones remains challenging. Existing multi-object tracking (MOT) methods [7], [15], [23]–[26] are generally effective only in simple scenarios with few and relatively large targets, but their performance degrades severely in dense crowds and under complex motion. VIC methods [21], [27], [28] are proposed to decompose video-level counting into estimating the number of pedestrians in the initial frame and the inflow pedestrian count for each subsequent frame. However, current methods heavily rely on accurate localization and strict one-to-one association, which are extremely difficult in dense crowds. As a result, localization and association errors accumulate and significantly degrade counting accuracy. Although density map-based VIC methods [29], [30] partially alleviate this issue, directly regressing the inflow, outflow, or shared density map remains challenging and lacks interpretability. Moreover, methods that compute cross-attention between feature maps of adjacent frames to estimate inflow density map [29], [31]

This work was supported in part by the JC STEM Lab of AI for Science and Engineering, funded by The Hong Kong Jockey Club Charities Trust, in part by the MTR Research Funding (MRF) Scheme under Grant CHU-24003, and in part by the Research Grants Council of Hong Kong under Project CUHK14213224. *(Corresponding author: Andy J. Ma.)*

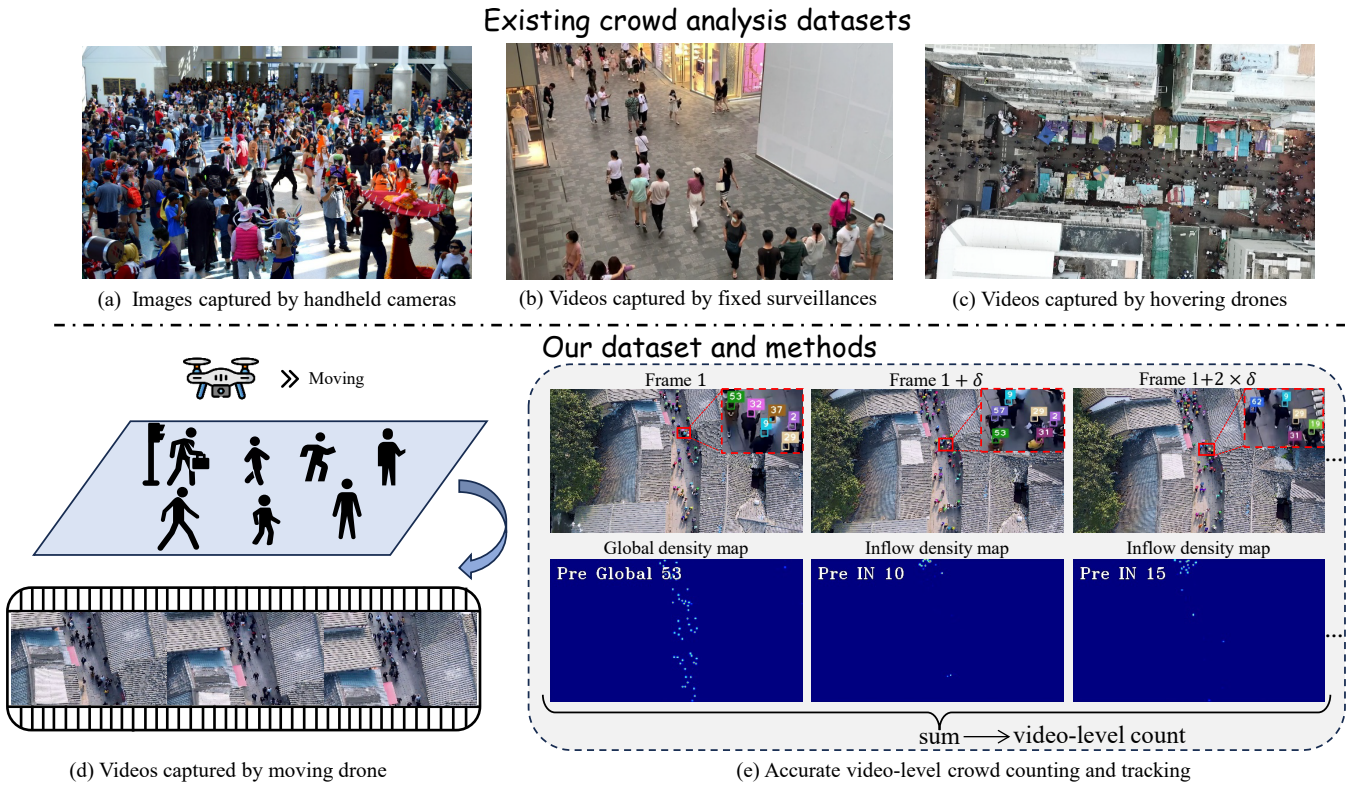
Yaowu Fan and Andy J. Ma are with the School of Computer Science and Engineering, Sun Yat-sen University.

Tao Han is with the school of Computer Science and Engineering, Hong Kong University of Science and Technology.

Antoni B. Chan is with the Department of Computer Science, City University of Hong Kong.

Jia Wan is with the School of Computer Science and Technology, Harbin Institute of Technology (Shenzhen).

W. Ouyang is with the Chinese University of Hong Kong.



(a) Images captured by handheld cameras (b) Videos captured by fixed surveillances (c) Videos captured by hovering drones

(d) Videos captured by moving drone (e) Accurate video-level crowd counting and tracking

Fig. 1. Comparison between existing crowd analysis datasets and ours. Existing research has predominantly focused on (a) free-viewpoint images captured by handheld cameras, (b) videos captured by fixed surveillance, or (c) hovering drones. Due to the constraints of these data acquisition setups, prior methods cannot perform video-level crowd counting and tracking in large-scale, crowded environments. Our method utilizes moving drones to capture videos covering large-scale scenes (d) and achieves accurate and interpretable video-level crowd counting and tracking (e).

incur high computational costs, making them unsuitable for efficient deployment in real-world applications.

In this paper, we study a practical yet underexplored problem: "***How to achieve accurate and efficient crowd counting and tracking in complex, large-scale scenes with dense crowds?***" To address this and overcome the aforementioned limitations, we first introduce a new large-scale dataset for video individual counting and tracking from moving drone perspectives in large-scale scenes with dense crowds. Unlike previous datasets that are constrained by limited fields of view or simple acquisition conditions, MovingDroneCrowd++ exhibits three key characteristics: high dynamics, dense crowds, and diverse and complex acquisition conditions. It encompasses various lighting conditions, shooting angles, and flight altitudes, bridging the domain gap and capturing the true complexity of real-world environments to support model training and evaluation (see Fig. 1 (d) and Fig. 2).

Due to the diversity and complexity of our dataset, existing counting and tracking methods struggle to handle its challenging scenarios effectively. To address the error accumulation of localization-based methods and the limited interpretability and high computational cost of existing density map-based approaches, we propose **GD^{3}A** (**G**lobal **D**ensity map **D**ecomposition via group-wise **D**escriptor **A**ssociation), an accurate, efficient, and interpretable density map-based VIC algorithm. Specifically, GD^{3}A first uses the global density map to filter out irrelevant background descriptors and retain multiple descriptors around each pedestrian head. It then performs pixel-level matching between pedestrian descriptors across adjacent frames via optimal transport [32] with an adaptive dustbin score. Based on the pixel-level matching, GD^{3}A decomposes the global density map of each frame into inflow, outflow, and shared density maps through robust group-wise association. By removing background descriptors, GD^{3}A substantially reduces computational complexity. Meanwhile, compared with existing strict one-to-one matching methods, group-wise association with multiple descriptors improves robustness: intra-group matching errors do not affect the final results, while inter-group errors are reduced from the instance level to the pixel level, effectively alleviating error accumulation. Therefore, our method is highly tolerant to localization and association errors. Moreover, the adaptive dustbin score computes a frame-pair-specific soft matching threshold, further improving association accuracy.

Furthermore, accurately tracking individuals in such dense and dynamic environments remains a formidable challenge. Building upon the robust group-wise association, we introduce a multi-object tracking method termed **DVTrack** (Descriptor Voting Track) without extra training. By performing a voting mechanism over pedestrian descriptors across adjacent frames, DVTrack converts pixel-level descriptor matches into instance-level pedestrian associations. Consequently, DVTrack naturally inherits the desirable properties of GD^{3}A, enabling efficient and accurate tracking of dense pedestrians in highly dynamic drone scenarios. Our methods perform counting and tracking based on the matching and voting results of multiple descriptors for each pedestrian. Intuitively, compared with matching based on a single vector per pedestrian, this design

is more robust and reliable, leading to more accurate results and less error accumulation across frames.

The contributions of this paper are summarized as follows:

- We introduce MovingDroneCrowd++, the largest and most challenging dataset to date specifically designed for video individual counting and tracking in large-scale crowded scenes captured by moving drones under diverse heights, angles, and lighting conditions.
- We propose GD^{3}A, which enables efficient and accurate VIC in challenging moving-drone scenarios with dense crowds by decomposing global density maps in an interpretable manner. This decomposition is achieved through robust group-wise descriptor association built upon optimal transport with an adaptive dustbin score.
- Based on the group-wise descriptor association, we further propose DVTrack. Without additional training, it converts pixel-level matching into instance-level associations via a voting mechanism, delivering superior tracking performance for dense pedestrians under highly dynamic drone motion.
- Extensive experiments demonstrate the superiority of our methods. GD^{3}A and DVTrack substantially outperform previous methods in moving drone scenarios with dense crowds and complex motions, reducing the counting error by 47.4% and improving tracking performance by 64.6%.

This work extends our preliminary research [29] in four key aspects: 1) First, we double the size of the original dataset by incorporating large-scale, densely crowded, and low-light scenes. This expansion creates a more diverse and challenging benchmark that accurately represents the complexity of real-world environments with dense crowds. 2) Second, we propose GD^{3}A, which achieves efficient and accurate VIC by global density map decomposition through group-wise association based on pixel-level descriptor matching. GD^{3}A achieves superior performance, higher computational efficiency, and improved interpretability compared to the SDNet proposed in [29]. 3) Third, based on GD^{3}A, we further introduce DVTrack, which achieves state-of-the-art dense crowd tracking in moving drone scenarios through a descriptor voting mechanism without extra training. 4) Finally, we conducted more comprehensive experiments and qualitative visualizations to validate the effectiveness and interpretability of the proposed methods. The results demonstrate that our methods significantly outperform prior works in both video individual counting and tracking (reducing the counting error by 47.4% and improving tracking performance by 64.6%).

II. Related Work

A. Image-level Crowd Counting

Image-level crowd counting aims to estimate the number of people in a given static image [4], [11], [33]–[37]. As a fundamental task in computer vision, it plays a crucial role in many real-world applications. This field has undergone substantial evolution and development over the past several years. In the early stages, detection-based methods [38] were sufficient for crowd counting in sparse scenarios. To better tackle dense crowd scenarios, regression-based approaches [3], [39] were subsequently introduced. With the prevalence of data-driven deep learning, datasets featuring extremely dense crowds have been introduced [9], [10], [12], [13]. Density map estimation-based methods [11], [33], which exhibit superior performance in such highly crowded scenes, have consequently become the dominant approach. As the complexity of the data increased, the field began to face several new challenges, including perspective effects [34], [40], head scale differences [36], [41], and domain gaps [42]–[44]. Moreover, researchers have proposed new loss functions [35], [45], [46], network architectures [5], [47], and supervision strategies [48]–[51]. Multi-view crowd counting [52], [53] extends crowd counting to larger-scale scenes to some extent, but it is still limited to fixed locations. Recently, Embodied Crowd Counting (ECC) [54] has been proposed for actively counting pedestrians in large-scale scenes. However, existing ECC methods rely on synthetic data and suffer from a significant domain gap with complex real-world environments, which limits their application. Although these studies have significantly advanced image-level crowd counting, the limited field of view and inflexibility of static images greatly constrain their applicability in the real-world, particularly in large-scale scenes with dense crowds.

B. Video-level Crowd Counting and Multi-Object Tracking

Video-level crowd counting [21], [27]–[31], defined as Video Individual Counting (VIC) in [27], aims to estimate the number of unique pedestrians across an entire video. [27] first modeled this task as predicting the number of pedestrians in the first frame and the inflow count in each subsequent frame. [21] proposed a weakly supervised approach that guides the learning process using predicted similarity. Other works have introduced density map-based methods [29]–[31], with [30] directly predicting inflow and outflow density maps, while [29] first predicts shared density maps and then derives the inflow and outflow density maps by subtracting the shared density maps from the global density maps. Localization-based methods rely on precise localization and strict one-to-one association, whereas density map-based methods either suffer from poor interpretability or incur high computational costs due to cross-frame attention. In contrast, multi-object tracking [55]–[57] is a classical task, whose common paradigm is tracking-by-detection [7], [58]–[60], where detection results are associated with historical trajectories using Kalman filtering [61]. Recently, some methods [7], [24], [62] have adopted Transformer and employ track queries to track targets. However, these methods cannot effectively handle dense crowds and fast drone motion. In contrast, our methods conduct robust group-wise descriptor association, which exhibits strong tolerance to errors in dense scenes and complex conditions.

C. Drone-based Crowd Counting and Tracking

To overcome the limitations of ground-based cameras, such as handheld devices and surveillance cameras, drones have also been employed in crowd counting and tracking due to their high flexibility [19], [20], [63]–[69]. However, these methods remain confined to image-level crowd counting [63], [66] or tracking on fixed-view videos captured by hovering drones [68], [69]. UAVVIC [21] contains only a small



Fig. 2. Exemplars from the MovingDroneCrowd++ dataset. Due to space constraints, only two frames are displayed for each video clip. Each frame is annotated with a bounding box and an identity ID for every pedestrian head. These examples illustrate that the dataset is captured by moving drones in dense crowd environments and exhibits significant diversity in terms of shooting angles, flight altitudes, and illumination conditions.

number of videos captured by moving drones, with most clips recorded in suburban areas featuring sparse crowds and limited variations in camera angle, altitude, and illumination. Consequently, it shows a substantial domain gap from real-world dense crowd scenarios. VisDrone [22] is a large-scale MOT dataset, but dense crowds are deliberately annotated as ignore regions. Our conference paper [29] introduces MovingDroneCrowd, a video dataset captured by moving drones in complex environments with dense crowds, featuring diverse variations in shooting angles, flight altitudes, and illumination conditions. However, it remains limited in scale and lacks large-scale, long-duration videos, making it insufficient for thoroughly evaluating the performance of different algorithms. MovingDroneCrowd++ introduces longer dynamic drone videos and doubles the size of MovingDroneCrowd, making it the largest and most challenging dynamic drone video dataset for dense crowd scenarios to date.

III. MovingDroneCrowd++

A. Data Collection and Processing

1) Collection: Due to the strict regulations on drone operations in crowded environments, acquiring dynamic drone video data in these areas presents a significant challenge, particularly in the highly congested scenarios targeted in this work, such as commercial districts, pedestrian streets, and tourist attractions. To this end, we curated publicly available drone videos depicting crowded outdoor public spaces. Candidate raw videos were identified through publicly accessible video platforms and search engines using crowd-related aerial-view keywords, such as "aerial crowd," "aerial pedestrian street," and "aerial tourist attractions". Subsequently, we selected and downloaded videos that adhere to the following criteria: 1) The video clips must be captured by moving drones in crowded scenes. 2) The video content must be pedestrian-centric with distinguishable head features. This necessitates a moderate flight altitude and a sufficient depression angle to reduce occlusion.

2) Processing: For the downloaded videos, we first used Boilsoft Video Splitter to segment them into multiple continuous clips, with each clip covering a specific region as completely as possible. Videos that were already continuous and coherent were left unsegmented. Note that the clips extracted from the same original video are grouped into the same scene. This is because these clips are typically captured in the same or nearby areas under similar collection conditions, resulting in a consistent domain style. Subsequently, to eliminate redundancy and reduce annotation costs, we performed frame sampling on each clip. However, since the drone flight speeds varied across the original videos, we adjusted the sampling rate accordingly and downsampled the frame rate by factors of 3, 6, or 9, depending on the drone's motion speed in each clip. Finally, for clips with small depression angles, we cropped each frame around its center with a smaller resolution. This removes distant regions where pedestrians are difficult to distinguish, which simultaneously reduces annotation difficulty and uncertainty while increasing the amount of pedestrian inflow. In general, this cropping operation has little impact on the total number of people in the clip, since pedestrians that are cropped will re-enter the field of view as the drone moves forward.

B. Dataset Annotation and Split

1) Instance-level Annotations: After completing the data collection and processing described above, the obtained video frames were assigned to 20 experienced annotators. During the annotation process, the annotators annotated each pedestrian starting from the first frame in which the individual appeared. They labeled head bounding boxes that tightly enclose the head and assigned a unique identity across the entire clip, continuing the annotation until the pedestrian completely exited the view. If the pedestrian's head became occluded, annotation was temporarily suspended, and the same identity was reassigned once the pedestrian reappeared. A video clip is considered fully annotated once all pedestrians with distinct identities have been completely annotated from their first to their last visible frame.

TABLE I

COMPARISON WITH RELATED DATASETS. MOVINGDRONECROWD++ IS THE LARGEST DATASET DEDICATED TO VIDEO INDIVIDUAL COUNTING AND TRACKING IN MOVING DRONES SCENARIOS WITH DENSE CROWDS. IT EXHIBITS THE MOST SIGNIFICANT DIVERSITY IN SHOOTING ANGLES, ALTITUDES, AND ILLUMINATION CONDITIONS. THESE FACTORS, COMBINED WITH ITS HIGH DYNAMIC CHARACTERISTICS, MAKE IT HIGHLY CHALLENGING.

Dataset	Perspective	Resolution	Moving	Images	Dynamic Frames	Scenes	Boxes	Tracks	Light	Height	Angle	IDs
CroHD [70]	Surveillance	1080P	✗	11,464	0	5	1,188,496	2,752	day&night	Fixed	Fixed	✓
VSCrowd [14]	Surveillance	4K-360P	✗	62,938	0	153	2,011,551	43,179	day&night	Fixed	Fixed	✓
WuhanMetroCrowd [18]	Surveillance	1080P-720P	✗	11,925	0	15	223,662	–	–	Fixed	Fixed	✗
DroneCrowd [19]	Drone	1080P	✗	33,600	0	25	4,864,280	20,800	day&night	Fixed	Fixed	✓
VisDrone [22]	Drone	4K-360P	✓	33,682	64%	57	519,196	3,976	day&night	∼ 10m	∼ 45-90°	✓
UAVVIC [21]	Drone	4K-1080P	✓	5,396	51%	24	398,158	–	day	∼ 20m	∼ 90°	✗
MovingDroneCrowd [29]	Drone	4K-720P	✓	4,940	100%	26	325,542	16,154	day&night	∼ 3-20m	∼ 45-90°	✓
MovingDroneCrowd++	Drone	4K-720P	✓	7,197	100%	44	638,718	27,866	day&night	∼ 3-20m	∼ 45-90°	✓

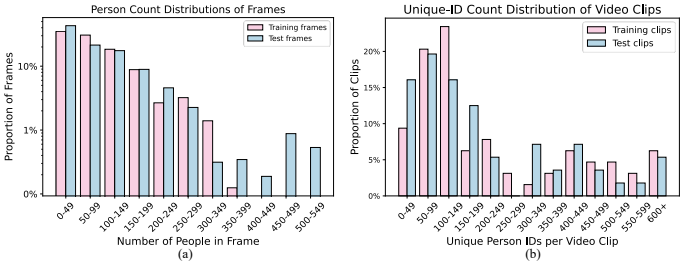


Fig. 3. Crowd density statistics of the MovingDroneCrowd++ dataset. (a) Histogram of people per frame. (b) Histogram of distinct identities per clip. These density statistics demonstrate the balance of the dataset split.

After the initial annotation of all video clips is completed, the annotations are reassigned to another group of annotators. For each trajectory, the inspection started from the first frame in which the pedestrian appeared and continued until the trajectory ended. Any errors identified during this process were recorded and corrected. Darklabel and CVAT were used for the annotation process, while TmoTA was employed for verification. TmoTA provides a visualization of all pedestrian trajectories and can highlight the selected trajectory, which greatly facilitates efficient and accurate error inspection.

2) Scene-level Annotations: In addition to the instance-level annotations, we also provide scene-level annotations for each video clip, including shooting time (daytime or nighttime), location, and difficulty level. The difficulty level is determined by the number of distinct pedestrians appearing in the entire clip, divided into four levels with intervals of 200 individuals. Moreover, compared to the conference version, the newly introduced video clips are additionally annotated with their durations. The scene-level annotations offer a principled foundation for both dataset splits and the evaluation of experimental results.

In total, we obtained **120** video clips from **44** distinct scenes, comprising **7,197** frames, **638,718** head bounding boxes, and **27,866** pedestrian trajectories. To the best of our knowledge, MovingDroneCrowd++ is not only the largest but also the most diverse and challenging dataset to date specifically designed for video individual counting and tracking in dense crowded scenes captured by moving drones.

3) Dataset Split: We split the dataset into training, validation, and test sets. Our dataset split has the following two important characteristics: **1) Scene-level Split**. This scene-level partition ensures that no video clips from the same or similar scenes appear across different subsets. This means that training and evaluation on our dataset are conducted in a cross-scene manner, which imposes a stronger requirement on the generalization capability of the algorithms. **2) Balanced Split**. With the scene-level annotations, we can perform a reasonable and balanced dataset split. This prevents undesirable biases, such as the training set contains most of the challenging scenes, while the test set mainly consists of simpler ones, which will distort evaluation results. Specifically, we split the dataset based on two main scene-level attributes: difficulty level and illumination. We first categorized all scenes according to these two key attributes and then randomly assigned the scenes within each category to the training, validation, and test sets following a predefined ratio.

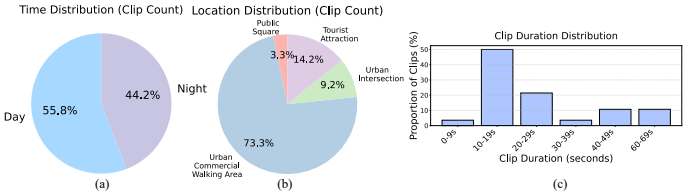


Fig. 4. Scene attributes statistics of the MovingDroneCrowd++ dataset. (a) Proportion of illumination conditions. (b) Proportion of shooting locations. (c) Duration histogram of the newly added clips. These scene attributes statistics highlight the diversity and challenging nature of the proposed dataset.

C. Dataset Statistical Analysis and Comparison

1) Statistical Analysis: Fig. 3 presents the count distribution of our dataset. Fig. 3(a) and Fig. 3(b) show the histograms of the number of pedestrians per frame and the number of distinct identities per video clip, respectively. As observed from these histograms, the distributions of the training and test sets are well balanced, enabling a fair and reliable evaluation of different algorithms. In addition, the histograms indicate that both the number of pedestrians per frame and the number of trajectories per clip are relatively dense. This demonstrates that our dataset effectively reflects the high-density pedestrian flows commonly observed in urban environments. Fig. 4(a) and Fig. 4(b) illustrate the distributions of shooting times and locations. Fig. 4(a) shows that the dataset contains a balanced number of videos captured during the daytime and at night. In particular, the inclusion of night-market scenes, which are classic examples of high-density pedestrian scenes under low-light conditions, further enhances the diversity and challenge of the dataset. Since pedestrian streets and commercial districts are difficult to distinguish clearly, we group them together as "Urban Commercial Walking Area." in Fig. 4(b). In addition, our dataset includes other typical high-density pedestrian areas, such as tourist attractions, intersections, and public squares. Finally, Fig. 4(c) presents the duration distribution of the newly added video clips. The distribution indicates that these new clips cover relatively large spatial areas, which further enriches the dataset.

2) Comparison: Table I presents a comparison between our dataset and other related video datasets. Although our dataset is not the largest in scale, it surpasses fixed-camera datasets in terms of dynamic motion and difficulty, offering a much broader spatial coverage. Compared with the other drone-based video dataset such as UAVVIC, our dataset has clear advantages in dynamic motion, scale, and diversity of shooting conditions, including scene types, shooting angles, flight altitudes, and illumination. It provides a more faithful representation of complex and crowded scenes in challenging dynamic drone scenarios. Moreover, the annotation of pedestrian trajectories in our dataset enables the training and evaluation of more advanced and powerful algorithms.

IV. Methodology

A. Problem Formulation and Overall Framework

Given a video clip $V = \{F_i\}_{i=1}^{n}$ captured by a moving drone in a scene with dense crowds, the goal is to count the number of unique pedestrians $M(V)$ appearing throughout the clip and track each pedestrian. For counting, we estimate the global density map $\hat{\mathbf{D}}_1^g$ of the first frame F_1 and the inflow density maps $\hat{\mathbf{D}}_i^{in}$ for all subsequent frames. The global density map $\hat{\mathbf{D}}_t^g$ contains the density values of all pedestrians in frame F_t, whereas the inflow density map $\hat{\mathbf{D}}_t^{in}$ contains the density values of pedestrians that newly appear in F_t. $M(V)$ can then be computed using the following formulation:

$$M(V) \approx \text{sum}(\hat{\mathbf{D}}_1^g) + \sum_{k=1}^{(n/\delta)-1} \text{sum}(\hat{\mathbf{D}}_{1+k\times\delta}^{in}), \tag{1}$$

where δ denotes the sampling interval between frames. For tracking, it needs to determine the position coordinates and identity of each pedestrian in every frame.

The overall pipeline of GD^{3}A is illustrated in Fig. 5. The training set $\mathcal{V} = \{V_j, P_j, ID_j\}_{j=1}^{m}$ consists of m video clips V_j along with their corresponding annotations. The annotations include the coordinates of pedestrians' head P_j in each frame and their unique identity ID_j throughout the entire video clip. During training, frames F_t and $F_{t+\delta}$ are sampled from a video clip V_j with a random interval δ. The feature maps $\mathbf{F}_t$ and $\mathbf{F}_{t+\delta}$, as well as the global density maps $\hat{\mathbf{D}}_t^g$ and $\hat{\mathbf{D}}_{t+\delta}^g$, are then obtained using the backbone and a pre-trained image-level density estimation model, respectively. The feature maps are first filtered using the global density maps to retain visual descriptors $\{\mathbf{f}_i^t\}_{i=1}^{N}$ and $\{\mathbf{f}_i^{t+\delta}\}_{i=1}^{M}$ for each pedestrian head in each frame. Note that a group of multiple visual descriptors, rather than a single descriptor, is retained for each pedestrian head. These visual descriptors are then enhanced using position. The enhanced descriptors are processed by an Attentional Graph Neural Network (AGNN) [71] to obtain association descriptors $\{\mathbf{d}_i^t\}_{i=1}^{N}$ and $\{\mathbf{d}_i^{t+\delta}\}_{i=1}^{M}$. Association descriptors from the two frames, together with the dustbin query, are fed into the dustbin score predictor to obtain an adaptive dustbin score s. Optimal transport then incorporates this adaptive dustbin score s to solve optimal matching matrix $\mathbf{P}^*$ between association descriptors.

Finally, based on $\mathbf{P}^*$, group-wise association is conducted and the global density map $\hat{\mathbf{D}}_t^g$ is decoupled into the shared density map $\hat{\mathbf{D}}_t^s$ and the outflow density map $\hat{\mathbf{D}}_t^o$. Similarly, $\hat{\mathbf{D}}_{t+\delta}^g$ is decomposed into the shared density map $\hat{\mathbf{D}}_{t+\delta}^s$ and the inflow density map $\hat{\mathbf{D}}_{t+\delta}^{in}$. The shared density map $\hat{\mathbf{D}}_t^s$ ($\hat{\mathbf{D}}_{t+\delta}^s$) represents pedestrians that appear in both frames F_t and $F_{t+\delta}$. The outflow density map $\hat{\mathbf{D}}_t^o$ contains pedestrians present in F_t but absent in $F_{t+\delta}$. Note that the shared and outflow density maps are byproducts, and only the inflow density map is useful. For tracking, pedestrian coordinates are obtained by detecting local maxima in the global density map. Based on the group-wise descriptor association established in GD^{3}A, DVTrack then employed a descriptor voting mechanism to convert pixel-level descriptor matches into instance-level pedestrian associations. Next, we provide a detailed description of each component.

B. Density Map Decomposition via Descriptor Association

1) Descriptor Extraction and Enhancement: For two given consecutive frames F_t and $F_{t+\delta}$, their feature maps are extracted by the backbone:

$$\mathbf{F}_t = \text{backbone}(F_t), \quad \mathbf{F}_{t+\delta} = \text{backbone}(F_{t+\delta}). \tag{2}$$

The dimensions of the feature maps $\mathbf{F}_t$ and $\mathbf{F}_{t+\delta}$ are $\mathbb{R}^{\frac{H}{r}\times\frac{W}{r}}$, where H and W are the height and width of the input frame, and r is the downsampling rate. Each feature map contains $\frac{H}{r}\times\frac{W}{r}$ visual descriptors. Associating all descriptors across two frames incurs prohibitive computational costs, and most descriptors correspond to the background regions, making their involvement unnecessary. Thus, we filter the feature maps using predicted global density maps obtained through a pre-trained image-level counter:

$$\hat{\mathbf{D}}_t^g = \text{counter}(F_t), \quad \hat{\mathbf{D}}_{t+\delta}^g = \text{counter}(F_{t+\delta}). \tag{3}$$

The filter process can be described as:

$$\mathbf{F}' = \mathbf{F} \odot \mathbb{I}(\hat{\mathbf{D}}^g > \tau), \tag{4}$$

where $\mathbb{I}$ is the indicator function and τ is the pre-defined threshold. Filtered feature maps $\mathbf{F}'_t$ and $\mathbf{F}'_{t+\delta}$ only contain visual descriptors of pedestrian heads, and the association of these descriptors significantly reduces the computational cost.

Formally, we define the set $\mathcal{A}_t = \{\mathbf{f}_i^t, \mathbf{p}_i^t\}_i^N$, where each $\mathbf{f}_i^t \in \mathbb{R}^D$ is a non-zero descriptor in $\mathbf{F}'_t$, and $\mathbf{p}_i^t = (x_i^t, y_i^t)$ is the coordinate of $\mathbf{f}_i^t$ in $\mathbf{F}'_t$. Similarly, $\mathcal{B}_{t+\delta} = \{\mathbf{f}_i^{t+\delta}, \mathbf{p}_i^{t+\delta}\}_i^M$ denotes the corresponding set constructed from $\mathbf{F}'_{t+\delta}$.

Due to the high similarity of pedestrian head appearances, accurately associating descriptors belonging to the same pedestrian across two frames is challenging. Therefore, visual descriptors are first enriched with spatial positions, as the same pedestrian typically appears at nearby locations in adjacent frames. To this end, an encoder is utilized to project the 2D vector (x_i^t, y_i^t) into the same feature space as the visual descriptor $\mathbf{f}$, and then the element-wise addition is performed between the projected vector and the visual descriptor:

$${}^{(0)}\mathbf{f}_i^t = \mathbf{f}_i^t \oplus \text{Encoder}(x_i^t, y_i^t). \tag{5}$$

To further enhance the distinctiveness of the descriptors, we use an AGNN to aggregate spatial and visual contextual cues via an iterative message-passing mechanism, which alternates

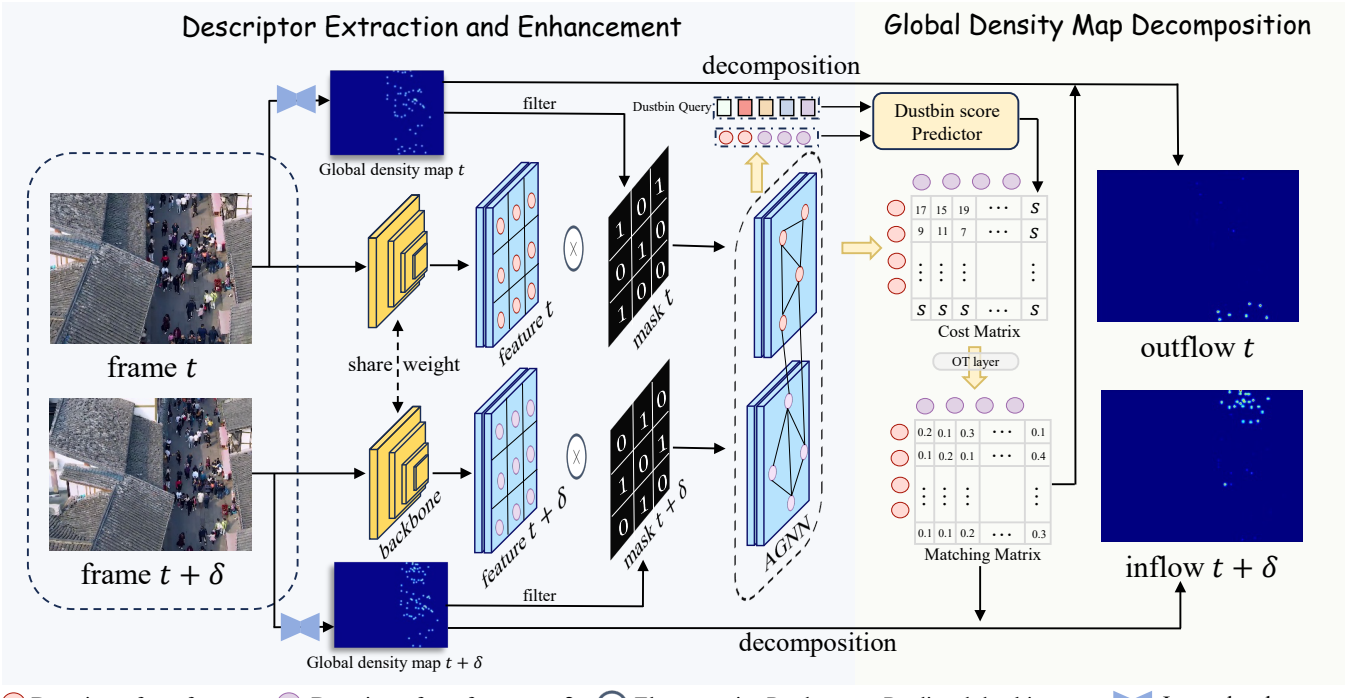


Fig. 5. The pipeline of the proposed GD^{3}A. Given two frames F_t and $F_{t+\delta}$, a backbone extracts feature maps $\mathbf{F}_t$ and $\mathbf{F}_{t+\delta}$, which are filtered using global density maps $\hat{\mathbf{D}}^g_t$ and $\hat{\mathbf{D}}^g_{t+\delta}$ predicted by a pre-trained image-level estimator to retain visual descriptors for pedestrian heads. Subsequently, these descriptors are enhanced with positional coordinates and refined by an AGNN for contextual aggregation. Pixel-level matching between descriptors from two frames are established via Optimal Transport with an adaptive dustbin score s, predicted by a dustbin score predictor. Finally, the global density map of each frame is decomposed into shared density map $\hat{\mathbf{D}}^s_t$ and $\hat{\mathbf{D}}^s_{t+\delta}$ (not visualized) and outflow/inflow density maps $\hat{\mathbf{D}}^o_t$ and $\hat{\mathbf{D}}^{in}_{t+\delta}$ through group-wise association.

between intra-image self-attention to encode local relationships and inter-image cross-attention to resolve matching ambiguities. The computation of the i-th descriptor at the l-th layer is:

$$ {}^{(l+1)}\mathbf{f}_i^t = {}^{(l)}\mathbf{f}_i^t + \mathrm{MLP}([{}^{(l)}\mathbf{f}_i^t || {}^{(l)}\tilde{\mathbf{f}}]), \tag{6} $$

where ${}^{(l)}\tilde{\mathbf{f}}$ is the message aggregated from other descriptors of the current frame or adjacent frame:

$$ \begin{aligned} \mathbf{Q} &= {}^{(l)}\mathbf{f}_i^t \mathbf{W}^Q, \quad \mathbf{K} = \tilde{\mathbf{F}}_\theta^l \mathbf{W}^K, \quad \mathbf{V} = \tilde{\mathbf{F}}_\theta^l \mathbf{W}^V, \\ {}^{(l)}\tilde{\mathbf{f}} &= \mathrm{Softmax}(\frac{\mathbf{Q}\mathbf{K}^T}{\sqrt{D}})\mathbf{V}, \end{aligned} \tag{7} $$

where $\mathbf{W}$ represents the learnable parameters at each layer. Note that each layer has its own learnable parameters, but the superscript l on $\mathbf{W}$ is omitted for brevity. $\tilde{\mathbf{F}}_\theta^l$ is the matrix obtained by concatenating all descriptors from the l-th layer of the current frame or adjacent frame. When l is even, θ is set to t, and $\tilde{\mathbf{F}}_t^l = [{}^{(l)}\mathbf{f}_0^t; {}^{(l)}\mathbf{f}_1^t; ...; {}^{(l)}\mathbf{f}_{N-1}^t]$. When l is odd, θ is set to $t+\delta$, and $\tilde{\mathbf{F}}_{t+\delta}^l = [{}^{(l)}\mathbf{f}_0^{t+\delta}; {}^{(l)}\mathbf{f}_1^{t+\delta}; ...; {}^{(l)}\mathbf{f}_{M-1}^{t+\delta}]$. Thus, Eq. 7 alternately apply self-attention and cross-attention to aggregate information from descriptors in the current frame or the neighboring frame. After passing through L layers, the output features ${}^{(L)}\mathbf{f}_i^t$ and ${}^{(L)}\mathbf{f}_i^{t+\delta}$ are obtained, which are then fed into a linear layer to produce the final descriptors for association:

$$ \mathbf{d}_i^t = \mathrm{MLP}({}^{(L)}\mathbf{f}_i^t), \quad \mathbf{d}_i^{t+\delta} = \mathrm{MLP}({}^{(L)}\mathbf{f}_i^{t+\delta}). \tag{8} $$

2) Pixel-level Descriptor Matching via OT with Adaptive Dustbin Score: Inspired by feature matching and graph matching [71], we perform augmented optimal transport on pixel-level descriptors for matching. An additional dustbin is introduced to match descriptors of inflow and outflow pedestrians that only appear in one frame. The dustbin score acts as a threshold to distinguish whether a descriptor corresponds to a pedestrian appearing in both frames. Previous methods typically learn a dustbin score for an entire dataset. However, such a strategy fails to account for the features of pedestrians in the current input, making it suboptimal. In contrast, we design a dustbin score predictor that outputs an optimal adaptive dustbin score conditioned on the pedestrian descriptors from the two input frames. Descriptor association can be formulated as **maximizing** the following objective:

$$ \begin{aligned} \mathrm{L}(\mathbf{a}, \mathbf{b}) &= \max_{\mathrm{P} \in \mathbf{U}(\mathbf{a},\mathbf{b})} < \mathbf{C}, \mathbf{P} > \\ &= \max_{\mathrm{P} \in \mathbf{U}(\mathbf{a},\mathbf{b})} \sum_{i \in [\![N+1]\!], j \in [\![M+1]\!]} \mathbf{C}_{i,j}\mathbf{P}_{i,j} \end{aligned} \tag{9} $$

where $\mathbf{C}$ is the cost matrix and is composed as:

$$ \mathbf{C} = \begin{bmatrix} \mathbf{S}_{N\times M} & \mathbf{s}_{N\times 1} \\ \mathbf{s}_{1\times M} & s \end{bmatrix}, \tag{10} $$

where $\mathbf{S}_{ij} = < \mathbf{d}_i^t, \mathbf{d}_j^{t+\delta} >$ is the similarity of the descriptors. $\mathbf{s}_{N\times 1}$, $\mathbf{s}_{1\times M}$, and s are filled with the optimal adaptive dustbin score s that is computed as:

$$ \begin{aligned} \mathbf{X}_{in} &= [\mathbf{q}, \mathbf{d}_1^t, \ldots, \mathbf{d}_N^t, \mathbf{q}, \mathbf{d}_1^{t+\delta}, \ldots, \mathbf{d}_M^{t+\delta}], \\ \mathbf{X}_{out} &= \mathrm{TransformerEncoder}(\mathbf{X}_{in}), \\ \mathbf{s}^1, \mathbf{s}^2 &= \mathbf{X}_{out}[1], \mathbf{X}_{out}[N+2], \\ s &= \mathrm{MLP}(\mathrm{Concat}(\mathbf{s}^1, \mathbf{s}^2)), \end{aligned} \tag{11} $$

where $\mathbf{q}$ is the learnable dustbin query.

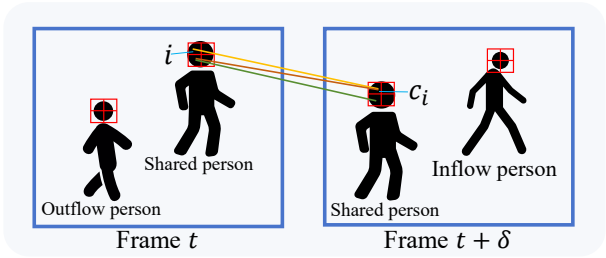


Fig. 6. Illustration of the group-wise association. For the i-th descriptor $\mathbf{f}_i^t$ in frame t, its highest matching score points to the c_i-th descriptor $\mathbf{f}_{c_i}^{t+\delta}$ in frame $t+\delta$. However, the best-matched descriptor of $\mathbf{f}_{c_i}^{t+\delta}$ in frame t may not be $\mathbf{f}_i^t$. We regard this match as valid if i is among the Top-K descriptors with the highest matching scores to $\mathbf{f}_{c_i}^{t+\delta}$, since intra-group matching errors do not affect the final counting and tracking results. By contrast, descriptors of inflow and outflow pedestrians fail to reach the predefined threshold and do not satisfy the reverse Top-K criterion. Their densities are therefore assigned to the inflow/outflow density maps.

In Eq. 9, $\mathbf{P}$ is the matching matrix to be solved, and the feasible set of $\mathbf{P}$ is defined as follows:

$$\mathbf{U}(\mathbf{a},\mathbf{b}) \overset{\text{def.}}{=} \{\mathbf{P} : \mathbf{P}\mathbb{1}_{M+1} = \mathbf{a} \text{ and } \mathbf{P}^\top \mathbb{1}_{N+1} = \mathbf{b}\}, \quad (12)$$

where $\mathbf{a}$ and $\mathbf{b}$ denote the marginal distributions, which are set as $\left[\mathbb{1}_N^\top, M\right]^\top$ and $\left[\mathbb{1}_M^\top, N\right]^\top$ for matching. For $i \le N$ and $j \le M$, $\mathbf{P}_{ij}$ is the probability of matching the i-th descriptor from frame t with the j-th descriptor from frame $t+\delta$. When $i = N+1$ and $j \le M$, $\mathbf{P}_{ij}$ represents the probability that the j-th descriptor in frame $t+\delta$ matches the dustbin (i.e., belongs to an inflow pedestrian), while for $j = M+1$ and $i \le N$, $\mathbf{P}_{ij}$ signifies the probability that the i-th descriptor in frame t matches the dustbin (i.e., belongs to an outflow pedestrian). Eq. 9 is essentially a linear programming problem with $N+M+2$ equality constraints, and the optimal matrix $\mathbf{P}^*$ can be obtained by Sinkhorn iteration [72].

3) Global Density Map Decomposition via Group-wise Association: By solving Eq. 9, the optimal matching matrix $\mathbf{P}^*$ is obtained. Based on $\mathbf{P}^*$, the predicted global density map can be decomposed into inflow, outflow, and shared density maps. Since each pedestrian head contains a group of multiple descriptors, it is reasonable that a descriptor at the center of a head in the current frame matches a descriptor located at the top-right of the same pedestrian's head in the adjacent frame. In other words, we allow matching errors within the descriptor group of each pedestrian, which improves robustness without compromising the accuracy of the final results. Based on this observation, we adopt a reverse top-K association strategy to implement group-wise association. The group size K is determined by the kernel size of the image-level density estimator and the downsampling ratio r, i.e., $K = (\text{kernel size}/r)^2$. Specifically, for the i-th descriptor $\mathbf{f}_i^t$ in frame F_t (the i-th row in $\mathbf{P}^*$), the column index of its maximum value is:

$$c_i = \arg\max_c \mathbf{P}^*_{ic}, \quad (13)$$

and the set of row indices corresponding to the top-K largest values of the column c_i is defined as:

$$\mathcal{R}^{c_i}_{topK} = \{r | r \in \{1,2,...,N\}, \mathbf{P}^*_{r,c_i} \ge v_K^{c_i}\}, \quad (14)$$

where $v_K^{c_i}$ is the K-th largest value in column c_i. An intuitive illustration of this process is provided in Figure 6. Based on

Algorithm 1 Pseudocode of GD^{3}A and DVTrack.

Require: Video frames F_t and $F_{t+\delta}$
Ensure: Inflow density map $\hat{\mathbf{D}}^{in}_{t+\delta}$, pedestrian trajectories

Stage 1: Descriptor Extraction and Enhancement
Extract features $\mathbf{F}_t, \mathbf{F}_{t+\delta}$ (Eq. 2) and global density maps $\hat{\mathbf{D}}^g_t, \hat{\mathbf{D}}^g_{t+\delta}$ (Eq. 3).
Filter features to obtain descriptor sets: $\mathcal{A}_t = \{\mathbf{f}_i^t, \mathbf{p}_i^t\}_{i=1}^N$ and $\mathcal{B}_{t+\delta} = \{\mathbf{f}_j^{t+\delta}, \mathbf{p}_j^{t+\delta}\}_{j=1}^M$.
Enhance descriptors to get $\mathbf{d}_i^t$ and $\mathbf{d}_j^{t+\delta}$ (Eq. 5–8).
Stage 2: Counting and Tracking via Group-wise Descriptor Association and Voting
Compute the adaptive dustbin score s (Eq. 11)
Construct the cost matrix $\mathbf{C}$ (Eq. 10)
Solve OT and obtain optimal matching matrix $\mathbf{P}^*$ (Eq. 9)
Get pedestrian positions $\{\tilde{\mathbf{p}}_k^t\}_{k=1}^{N_p}$ and $\{\tilde{\mathbf{p}}_k^{t+\delta}\}_{k=1}^{M_p}$.
Initialize voting matrix $\mathbf{V} \in \mathbb{R}^{N_p \times M_p}$ with zeros.
for each descriptor i in F_t (symmetrically for $F_{t+\delta}$) **do**
  Get match index c_i^* (Eq. 13–15).
  if $c_i^* \neq -1$ (Matched) **then**
    Assign corresponding density to *Shared* map.
    Identify pedestrian indices k_i and $k_{c_i^*}$ (Eq. 16).
    Vote: $\mathbf{V}_{k_i,k_{c_i^*}} \leftarrow \mathbf{V}_{k_i,k_{c_i^*}} + 1$.
  else
    Assign density to *Outflow* or *Inflow* density maps.
  end if
end for
Propagate IDs based on optimal associations in $\mathbf{V}$ and initialize new IDs for unmatched pedestrians.
return Inflow density map $\hat{\mathbf{D}}^{in}_{t+\delta}$, updated trajectories

Eq. 13 and 14, the index c_i^* of descriptor in $F_{t+\delta}$ matched to $\mathbf{f}_i^t$ can be obtained:

$$c_i^* = \begin{cases} c_i, & \text{if } i \in \mathcal{R}^{c_i}_{topK} \\ -1, & \text{otherwise} \end{cases} \quad (15)$$

if $c_i^* \neq -1$, the density value corresponding to $\mathbf{f}_i^t$ in the global density map $\hat{\mathbf{D}}^g_t$ is assigned to the shared density map $\hat{\mathbf{D}}^s_t$; otherwise, it is assigned to the outflow density map $\hat{\mathbf{D}}^o_t$. Similarly, global density map $\hat{\mathbf{D}}^g_{t+\delta}$ can be decomposed into shared density map $\hat{\mathbf{D}}^s_{t+\delta}$ and inflow density maps $\hat{\mathbf{D}}^{in}_{t+\delta}$.

C. Descriptor Voting Track

By detecting local maxima in the global density map $\hat{\mathbf{D}}^g_t$ and $\hat{\mathbf{D}}^g_{t+\delta}$ and extracting their corresponding coordinates $\{\tilde{\mathbf{p}}_k^t\}_{k=1}^{N_p}$ and $\{\tilde{\mathbf{p}}_k^{t+\delta}\}_{k=1}^{M_p}$, the positions of all pedestrians can be obtained, where N_p and M_p denote the numbers of pedestrians in frames t and $t+\delta$, respectively. For a descriptor in F_t or $F_{t+\delta}$, its corresponding pedestrian can be identified using the following formulation:

$$k_i = \arg\min_k d(\mathbf{p}_i, \tilde{\mathbf{p}}_k), \quad (16)$$

where d denotes the distance between two points. Let the voting matrix be $\mathbf{V} \in \mathbb{R}^{N_p \times M_p}$, for each descriptor $\mathbf{f}_i^t$ in frame F_t, we first obtain the index c_i^* of its matched descriptors in frame $F_{t+\delta}$ using Eq. 15. If $c_i^* \neq -1$, their corresponding pedestrian indices k_i and $k_{c_i^*}$ are then determined using Eq.

16, and the corresponding entry $\mathbf{V}_{k_i,k_{c_i^*}}$ in the voting matrix is incremented by one vote. By applying the same procedure to all descriptors $\mathbf{f}_j^{t+\delta}$ in $F_{t+\delta}$, the final voting matrix $\mathbf{V}$ is obtained. The Hungarian algorithm [73] is then applied to $\mathbf{V}$ to derive the pedestrian associations between the two frames. Based on these associations, pedestrian IDs from F_t are propagated to $F_{t+\delta}$, while new IDs are assigned to pedestrians in $F_{t+\delta}$ that remain unmatched (i.e., those with corresponding entries equal to 0 in the voting matrix $\mathbf{V}$). Algorithm 1 summarizes the execution process of GD^{3}A and DVTrack. Please refer to it for more details.

D. Loss Function

Since the dataset provides only the coordinates of pedestrian head centers and their corresponding identity labels, pixel-level descriptor correspondences are unavailable. Therefore, we first extend the point-level annotations to pixel-level annotations for the head regions based on local spatial correspondence. Assume that, for a given pedestrian, the head center is located at $\mathbf{p}_t$ in frame t and at $\mathbf{p}_{t+\delta}$ in frame $t+\delta$. Using local spatial correspondence, we can infer pixel-level correspondence for the surrounding local region based on a local displacement offset $\mathbf{\Delta} \in \mathbb{Z}^2$:

$$\mathbf{p}_t + \mathbf{\Delta} \longleftrightarrow \mathbf{p}_{t+\delta} + \mathbf{\Delta}, \forall \mathbf{\Delta} \in \mathbb{Z}^2, \|\mathbf{\Delta}\|_\infty < \rho, \tag{17}$$

where ρ is the pre-defined radius of the local region, and $\longleftrightarrow$ indicates that the descriptors at the two positions correspond to each other (i.e., the same local position of the same pedestrian head in two frames). Using the above extension, the indices of descriptors to be matched between the two frames are divided into three sets: $\mathcal{M}$, $\mathcal{U}_A$, and $\mathcal{U}_B$. $\mathcal{M} = \{(i,j)_k\}_{k=1}^{N_m}$ contains the indices of matched descriptors, $\mathcal{U}_A$ contains the indices of descriptors belonging to outflow pedestrians, and $\mathcal{U}_B$ contains the indices of descriptors belonging to inflow pedestrians. Finally, the loss can be computed as follows:

$$\begin{aligned}\mathcal{L} = &- \sum_{(i,j)\in\mathcal{M}} \log \mathbf{P}_{i,j} \\ &- \sum_{i\in\mathcal{U}_A} \log \mathbf{P}_{i,M+1} - \sum_{j\in\mathcal{U}_B} \log \mathbf{P}_{N+1,j},\end{aligned} \tag{18}$$

where $\mathbf{P}$ is the matrix obtained by solving Eq. 9.

Thanks to the differentiability of the optimal transport algorithm, backpropagation can be performed from the association stage to the backbone and the dustbin score predictor, thereby encouraging descriptors of the same pedestrian to be similar, those of different pedestrians to be dissimilar, and enabling the dustbin score predictor to learn an optimal adaptive dustbin score tailored to the input frame pair.

V. Experiments

This section first introduces the datasets and evaluation metrics used in our experiments, followed by the key implementation details. We then compare our method with various related approaches to demonstrate its superior performance. Ablation studies further verify the robustness of our method, and visualization comparisons intuitively highlight its interpretability compared to existing methods.

A. Experiment Setup

1) Datasets: To validate the effectiveness of the proposed method, we conduct experiments on both our MovingDroneCrowd++ captured by moving drones and the surveillance video dataset VSCrowd [14]. VSCrowd contains 634 video clips recorded by fixed surveillance cameras across 153 different scenes, with a resolution of 1920×1080 and a total of 62,938 frames. We adopt the same dataset split for training and evaluation in [27]. MovingDroneCrowd++ and VSCrowd provide sufficiently diverse data to enable a comprehensive evaluation of different approaches.

2) Evaluation Metric: The primary evaluation metrics for counting are video-level MAE and RMSE:

$$\text{MAE} = \frac{1}{N}\sum_{i=1}^{N}|y_i - \hat{y}_i|, \quad \text{RMSE} = \sqrt{\frac{1}{N}\sum_{i=1}^{N}(y_i - \hat{y}_i)^2}, \tag{19}$$

where y_i denotes the ground-truth count of distinct pedestrians in a video clip, $\hat{y}_i$ is the predicted count, and N is the number of video clips in test set. In addition, we adopt WRAE, MIAE, and MOAE defined in [27]. WRAE (Weighted Relative Absolute Errors) weights the relative error by the proportion of frames in each video clip, thereby accounting for the impact of video lengths. The previously mentioned metrics evaluate errors at the video level, whereas MIAE and MOAE measure the errors of pedestrian inflow and outflow at the frame pair level. For tracking, we adopt the widely used metric HOTA [74], which provides a balanced evaluation of detection (DetA) and association (AssA) accuracy. In addition, we also report the results of MOTA [75] and IDF1 [76].

3) Implementation Details: During training, the frame interval is randomly sampled to ensure diverse pedestrian motion patterns and varying drone speeds. In data augmentation, random horizontal flipping is not applied, as it would disrupt the positional consistency of the same pedestrian across frames. The cropping and scaling strategies follow [27]. We adopt ResNet50 [77] as the backbone network (initialized with weights pretrained on ImageNet), followed by an FPN [78] to enhance multi-scale representation. The initial learning rate is set to 5e-5 for the backbone and 1e-4 for the dustbin score predictor and AGNN. The model is implemented in PyTorch and trained on RTX 3090 with a global batch size of 8.

B. Comparison with State-of-the-Art Methods

In this subsection, we compare the proposed GD^{3}A and DVTrack with several representative SOTA methods on video individual counting and multi-object tracking tasks.

1) Comparison of Video Individual Counting on MovingDroneCrowd++: As shown in Table II, different types of methods are separated by horizontal lines. Multi-object tracking methods count pedestrians by tracking each individual in the video and using the number of resulting trajectories as the final count. However, multi-object tracking methods perform poorly on MovingDroneCrowd++, especially on highly challenging video clips, because they struggle to handle the dense crowd scenes and rapid drone motion in MovingDroneCrowd++. While VIC methods based on localization and cross-frame matching significantly outperform

TABLE II
COMPARATIVE RESULTS FOR VIDEO-LEVEL CROWD COUNTING ON MOVINGDRONECROWD++. CLIPS ARE DIVIDED INTO FOUR DIFFICULTY LEVELS $D_0 \sim D_3$ BASED ON THE NUMBER OF UNIQUE PEDESTRIAN, WITH THE TRAJECTORIES RANGES OF [0, 200), [200, 400), [400, 600), AND ≥ 600, RESPECTIVELY. OUR METHOD ACHIEVES THE BEST OVERALL PERFORMANCE, WITH CLEAR ADVANTAGES ON HIGH-DIFFICULTY CLIPS.

Method	Venue	MAE↓	RMSE↓	WRAE↓	MIAE↓	MOAE↓	Density levels			
							D_0	D_1	D_2	D_3
Multi-Object Tracking Methods										
ByteTrack [23]	ECCV'22	244.32	551.05	117.39	18.35	18.17	92.07	227.67	364.20	1448.00
BoT-SORT [58]	arXiv'22	278.02	589.75	132.99	20.92	20.80	131.41	215.83	368.80	1570.67
OC-SORT [60]	CVPR'23	188.49	308.74	75.85	10.43	11.27	61.89	268.17	423.00	777.67
DiffMOT [59]	CVPR'24	337.85	802.59	165.91	25.87	25.58	129.52	248.83	571.80	2001.00
MOTIP [7]	CVPR'25	116.61	215.57	47.72	8.87	8.03	51.37	103.33	163.20	652.67
Localization-based VIC Methods										
DRNet [27]	CVPR'22	83.04	172.07	30.88	8.60	7.96	28.23	96.41	160.67	420.20
CGNet [21]	CVPR'24	80.85	184.51	26.13	–	–	19.37	96.17	171.40	452.67
LOI [79]	ECCV'16	245.24	357.76	99.08	–	–	103.20	328.72	476.90	970.48
Density map-based VIC Methods										
FMDC [30]	WACV'24	127.78	208.82	46.22	7.69	7.44	46.10	190.62	235.93	556.93
SDNet [29] (Ours)	ICCV'25	76.24	160.33	32.40	6.40	6.08	31.87	88.84	143.68	337.96
GD^{3}A(Ours)	–	**40.11** ↓ 47.4%	**71.61** ↓ 55.3%	**18.83** ↓ 27.9%	**3.67** ↓ 42.7%	**3.47** ↓ 42.9%	**17.96** ↓ 7.3%	**66.30** ↓ 25.4%	**83.94** ↓ 41.6%	**114.10** ↓ 66.2%

TABLE III
COMPARISON OF MULTI-OBJECT TRACKING ON MOVINGDRONECROWD++. DVTRACK ACHIEVES THE BEST PERFORMANCE AND SIGNIFICANTLY OUTPERFORMS PREVIOUS METHODS.

Methods	Venue	HOTA ↑	DetA ↑	AssA ↑	MOTA ↑	IDF1 ↑
ByteTrack [23]	ECCV'22	17.5	20.8	17.1	5.0	11.7
BoT-SORT [58]	arXiv'22	17.5	20.8	16.9	4.8	11.4
OC-SORT [60]	CVPR'23	11.7	6.3	24.7	3.0	7.3
DiffMOT [59]	CVPR'24	20.9	28.2	17.6	4.6	14.2
MOTIP [7]	CVPR'25	11.2	14.3	10.0	-7.7	8.5
DVTrack(Ours)	–	**34.4** ↑ 64.6%	**29.4** ↑ 4.3%	**41.2** ↑ 66.8%	**12.8** ↑ 156%	**41.3** ↑ 190.8%

multi-object tracking, precise localization and strict one-to-one association remains challenging due to crowdedness, complex illumination, and the small scale of pedestrian heads. These localization and association errors limit the final counting accuracy. Density map-based VIC methods circumvent the need for explicit localization and association. FMDC directly predicts outflow and inflow density maps for two consecutive frames. However, due to the inherent difficulty of this paradigm, its performance is limited and even fall behind localization-based approaches. Our conference method, SDNet, alleviates task complexity by first estimating shared density maps and achieves the second-best performance among all compared methods, following our GD^{3}A. However, accurately estimating the density map between two frames is challenging. As time progresses, erroneous density estimates gradually accumulate, thereby degrading the final counting performance.

In contrast, our method GD^{3}A avoids the strict localization and one-to-one association process and achieves SOTA performance by decoupling global density maps into shared, outflow and inflow components via robust group-wise pixel-level pedestrian descriptor association using OT with an adaptive dustbin score. Notably, the performance gains become more pronounced as the video difficulty increases: compared with previous methods, GD^{3}A reduces the counting error by 41.6% and 66.2% on the high-difficulty subsets D_2 and D_3, respectively.

2) Comparison of Video Individual Crowd Counting on VSCrowd: In addition to experiments on our dynamic drone video dataset, we also compare our method with other approaches on large-scale surveillance video dataset VSCrowd. As illustrated in Table IV, our method achieves the best overall performance on datasets captured by fixed surveillance cameras. This indicates that our approach is effective not only in moving drone scenarios but also in static surveillance settings, highlighting its remarkable generalizability and robustness. On this dataset, the performance gap between our approach and existing methods is less pronounced, primarily because localization and one-to-one association is relatively easier from a fixed surveillance perspective. The reduced scene complexity allows localization-based methods to achieve competitive results with ours.

3) Comparison of Tracking on MovingDroneCrowd++: Table III presents a comparison between our method, DVTrack, and recent classical and state-of-the-art multi-object tracking methods on MovingDroneCrowd++. These methods include both end-to-end Transformer-based method and conventional tracking-by-detection methods. Experimental results demonstrate that our method significantly outperforms all competing methods in dense crowd scenarios captured by moving drones. Existing methods suffer from either poor detection performance or weak association capability under dense crowds with complex motion conditions. In particular, the Transformer-based MOT method MOTIP performs poorly because it relies on a predefined vocabulary size for identity representation, making it unsuitable for dense crowd scenarios in our dataset, where scaling the vocabulary size leads to prohibitive training costs. Overall, our method DVTrack achieves a 64.6% improvement in HOTA over the second-best method DiffMOT, highlighting its strong superiority in dense and complex motion scenarios.

TABLE IV
COMPARATIVE VIDEO-LEVEL CROWD COUNTING RESULTS ON SURVEILLANCE VIDEO DATASET VSCROWD DEMONSTRATE THAT OUR METHOD ACHIEVES THE BEST OVERALL PERFORMANCE. THIS INDICATES THAT OUR APPROACH PERFORMS WELL ON BOTH MOVING DRONE AND FIXED SURVEILLANCE SCENARIOS. D0 $\sim$ D4 DENOTE FIVE PEDESTRIAN DENSITY RANGE: [0, 50), [50, 100), [100, 150), [150, 200), $\geq$ 200, RESPECTIVELY.

Method	Venue	MAE↓	RMSE↓	WRAE(%)↓	MIAE↓	MOAE↓	Density levels				
							D_0	D_1	D_2	D_3	D_4
FairMOT [80]	IJCV'21	35.4	62.3	48.9	4.9	4.4	13.5	22.4	67.9	84.4	145.8
HeadHunter-T [70]	CVPR'21	30.0	50.6	38.6	4.0	4.1	11.8	25.7	56.0	92.6	131.4
LOI [79]	ECCV'16	24.7	33.1	37.4	–	–	12.5	25.4	39.3	39.6	86.7
DRNet [27]	CVPR'22	9.3	16.5	12.1	2.0	2.0	4.9	7.3	13.9	30.6	42.3
CGNet [21]	CVPR'24	8.9	17.7	12.6	–	–	5.0	5.8	**8.5**	25.0	63.4
PDTR [28]	MM'24	9.6	17.6	11.4	–	–	4.6	6.8	14.7	23.6	60.6
OMAN [81]	ICIP'25	8.3	15.4	11.1	–	–	3.9	6.2	13.2	20.3	48.2
SDNet [29] (Ours)	ICCV'25	8.6	15.9	11.0	–	–	4.0	6.6	12.6	24.9	**47.9**
GD^{3}A(Ours)	–	**7.5**	**15.4**	**8.9**	**1.7**	**1.8**	**3.3**	**5.1**	11.2	**17.3**	53.8

TABLE V
ABLATION STUDY ON THE EFFECTS OF PEDESTRIAN LOCATION, PEDESTRIAN DENSITY, AND AGNN DURING THE MATCHING PROCESS.

Position	Density	AGNN	MAE ↓	RMSE ↓	WRAE ↓
			71.37	120.03	34.14
✓			69.62	115.36	32.72
	✓		72.29	124.38	35.42
✓	✓		70.01	117.48	33.68
		✓	68.59	108.66	34.21
✓		✓	**66.13**	**101.70**	**30.50**
	✓	✓	69.90	123.88	31.88
✓	✓	✓	66.61	111.01	30.71

TABLE VI
ABLATION STUDY OF THE ADAPTIVE DUSTBIN SCORE ON THE VALIDATION SET OF MOVINGDRONECROWD++, WHERE ADS DENOTES THE ADAPTIVE DUSTBIN SCORE.

Method	ADS	MAE ↓	RMSE ↓	WRAE ↓
DRNet	✗	91.79	131.47	40.09
	✓	**77.71**	**120.65**	**27.91**
Ours	✗	54.14	102.23	23.82
	✓	**32.25**	**46.58**	**18.84**

TABLE VII
EFFECT OF GROUP-WISE ASSOCIATION AND DESCRIPTOR VOTING.

Group-wise Association					
Method	MAE ↓	RMSE ↓	WRAE ↓	MIAE ↓	MOAE ↓
GD^{3}A	**40.11**	**71.61**	**18.83**	**3.67**	**3.47**
GD^{3}A w/o Group-wise Association	129.98	236.87	58.43	10.10	9.56

Descriptor Voting Mechanism					
Method	HOTA ↑	DetA ↑	AssA ↑	MOTA ↑	IDF1 ↑
DVTrack	**34.4**	**29.4**	**41.2**	**12.8**	**41.3**
DVTrack w/o Voting	22.7	29.4	19.3	-7.2	20.2

C. Ablation Studies

1) Effect of Position and Density on the Association: We first conduct ablation studies on the pedestrian descriptor association process. Specifically, we examine the impact of incorporating auxiliary information, including pedestrian density values and spatial locations, as well as the effect of performing matching with or without contextual aggregation using an AGNN. As shown in Table V, we provide a detailed experimental analysis of these three factors during the matching process. It is evident that incorporating pedestrian locations and employing AGNN during the matching process both consistently improve performance, whereas introducing density values has a negative effect on performance. This can be intuitively explained. Each pedestrian has a unique spatial location, and the position of the same pedestrian typically changes slightly between adjacent frames, making location information highly discriminative for identity association. Furthermore, AGNN aggregates contextual information into each pedestrian descriptor, which further enhances the discriminability between descriptors belonging to different pedestrians. Density values cannot sufficiently capture pedestrian locations and appearance features, and the density values predicted by the pretrained model during test may introduce additional noise. Therefore, we ultimately use only positional information to enhance the visual descriptors.

2) Effect of Adaptive Dustbin Score: Table VI presents an ablation study on the effect of the adaptive dustbin score. We conduct experiments on the OT-based instance-level matching method DRNet and our pixel-level descriptor matching method GD^{3}A, comparing a dataset-level learnable dustbin score with the proposed adaptive dustbin score. The results show that using the adaptive dustbin score significantly improves the final counting performance. This indicates that the adaptive dustbin score can adaptively estimate an optimal dustbin score based on pedestrian features in the current frame pair, thereby effectively distinguishing shared pedestrians from inflow and outflow ones.

3) Effect of Group-wise Association and Descriptor Voting Mechanism: Table VII shows the effects of group-wise association in GD^{3}A and the descriptor voting mechanism in DVTrack. In GD^{3}A w/o Group-wise Association, we adopt a strict one-to-one association strategy similar to [27], which leads to a significant performance drop. This indicates that group-wise descriptor association is more suitable for dense crowds and complex illumination conditions, as its intra-group error tolerance effectively mitigates error accumulation. DVTrack w/o Voting directly matches the descriptors at peak points of pedestrian heads and transfers IDs across adjacent frames according to the matching results, resulting in a large drop in ID association metrics (AssA). This demonstrates that

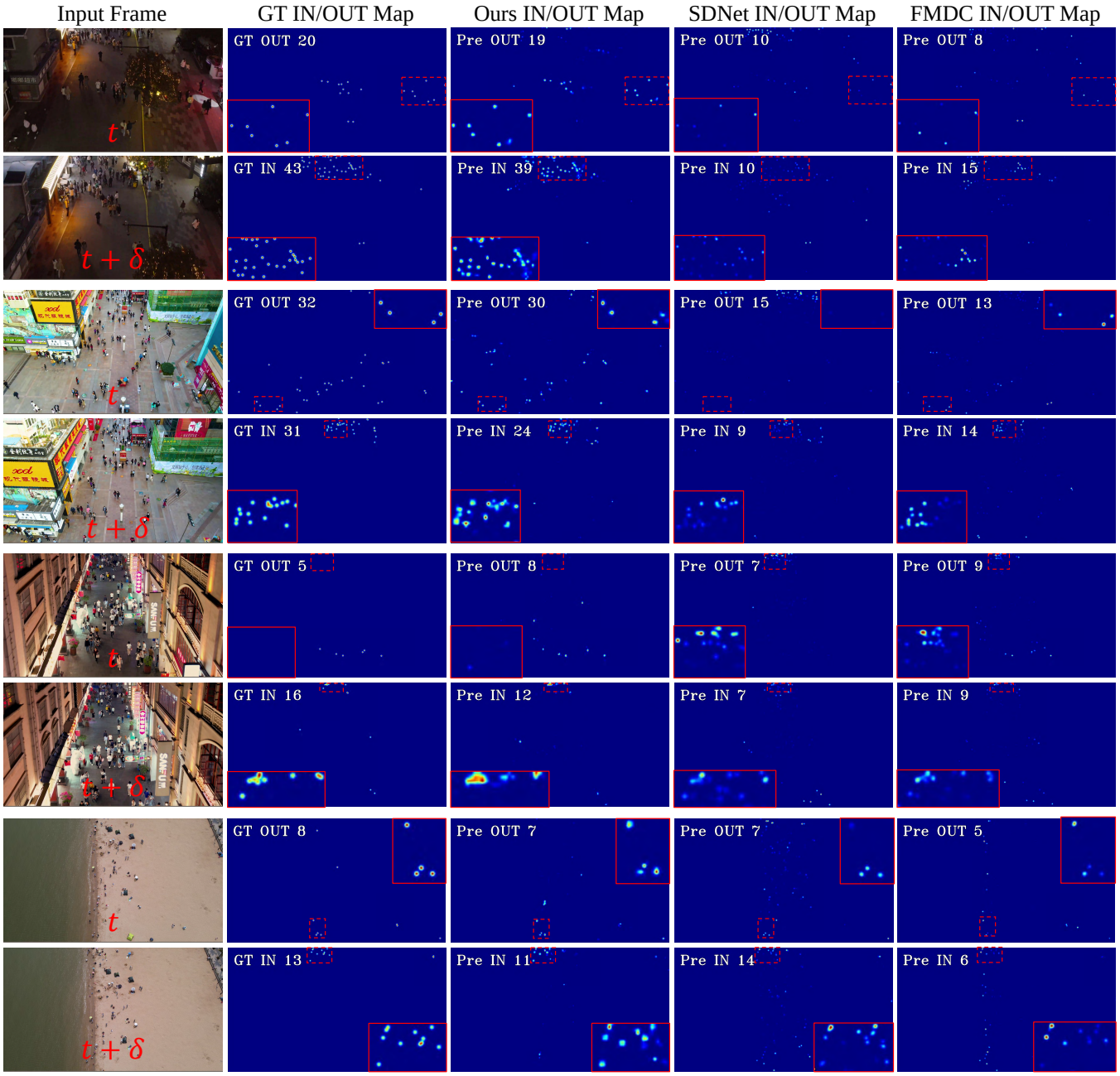


Fig. 7. Visual comparison of inflow and outflow density maps predicted by our method and other density map-based VIC methods. For each frame pair, the first row shows the outflow density maps, while the second row presents the inflow density maps. Compared with other methods, our approach more accurately predicts inflow and outflow counts and yields density maps that are more interpretable and more consistent with the ground-truth

our descriptor voting mechanism is more accurate and robust for ID association than directly relying on single-descriptor matching.

4) Effect of Frame Sampling Interval at Test Time: To evaluate the sensitivity of our method to temporal intervals and its performance under different drone movement speeds, we test our method and competing methods under frame sampling intervals ranging $0.04\,\mathrm{s}$ to $6\,\mathrm{s}$ with a step size of 0.04s. For our dataset captured by moving drones, this range covers a wide spectrum of temporal variations and thus provides a comprehensive evaluation. As shown in Fig. 8(a), our method exhibits stable performance across the entire interval range. In contrast, the other methods achieve their best performance at an interval of approximately 1 second, after which their performance degrades noticeably as the interval increases. This indicates that our method is robust to temporal variations at test time. Even with substantial variations in the frame interval, the performance remains stable without significant fluctuations. More importantly, it remains reliable when drones move at high speeds.

5) Trade-off between Performance and Efficiency: Fig. 8(b) illustrates the performance–efficiency trade-off. Our method achieves the best balance between performance and efficiency, delivering the highest accuracy while maintaining high computational efficiency. Compared with our conference method SDNet, which is based on cross-attention, GD^{3}A filters feature

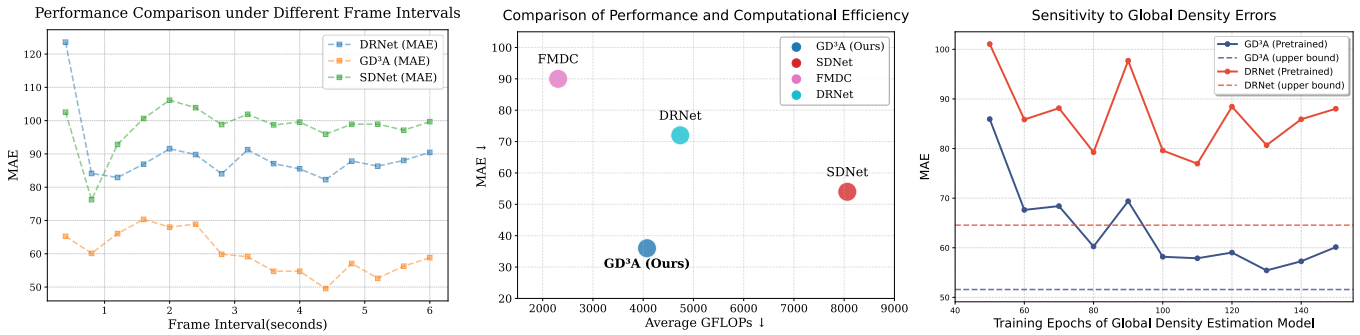


Fig. 8. (a) Comparison of our method with other methods under different frame intervals, ranging from 0.04 s to 6 s with a step size of 0.04 s. (b) Performance–efficiency trade-off comparison between our method and existing approaches. (c) Sensitivity analysis to errors in the predicted density maps for our method and other approaches.



Fig. 9. Visual comparisons of tracking results. Other methods suffer from frequent ID switches and localization errors, whereas our method DVTrack maintains more consistent identities. The enlarged white dashed boxes show the local details of the regions indicated by the solid white boxes.

maps using global density maps to exclude descriptors from dominant background regions. This significantly reduces redundant computations and improves computational efficiency.

6) Sensitivity to Global Density Estimation: Fig. 8(c) presents a sensitivity analysis of our method and the localization-based method DRNet with respect to the predicted global density maps. The red dashed line indicates the counting MAE of DRNet when ground-truth global density maps are provided at test time, which allows DRNet to use accurate pedestrian locations and thus eliminates localization errors (performance upper bound). The red solid lines denote the MAE of DRNet when using global density maps predicted by models trained for different numbers of epochs. As shown, the red solid line exhibits large fluctuations and a clear gap from the upper bound, indicating that localization-based methods are highly sensitive to the accuracy of density and localization predictions. In contrast, our method GD^{3}A (represented by the blue curves) is considerably more robust to density estimation errors, showing only a small performance gap between using predicted density maps and the upper-bound performance obtained using ground-truth density maps.

D. Qualitative Results

To intuitively demonstrate the superiority of our method over other methods, Fig. 7 presents a visual comparison of the inflow and outflow density maps predicted by our method and other density map-based VIC methods on two adjacent frames. For each frame pair, the first row shows the outflow density maps, while the second row presents the inflow density maps. The ground-truth or predicted inflow/outflow counts are presented in the top-left corner of each density map. Red dashed boxes indicate representative regions, while the red solid boxes show enlarged views of the corresponding regions. As can be observed, compared with other methods,

our approach achieves superior performance in terms of both the interpretability of the predicted inflow and outflow density maps and the accuracy of the corresponding inflow and outflow counts. This advantage stems from the fact that our method can more effectively distinguish between inflow and outflow pedestrians, whereas other methods struggle to do so, resulting in noisier predicted inflow and outflow density maps.

Fig. 9 presents qualitative comparisons between DVTrack and other SOTA multi-object tracking methods. As shown in the highlighted regions within the enlarged white dashed boxes, tracking-by-detection methods can detect more pedestrians but suffer from severe identity switches across frames due to the rapid motion of the drone. In contrast, transformer-based methods exhibit fewer identity switches but miss a large number of pedestrians. Our method detects most pedestrians while maintaining high identity consistency across frames. These results indicate that existing MOT methods degrade significantly under complex motion and dense crowd conditions, whereas our approach handles such scenarios more effectively.

VI. Conclusion

This paper presents a benchmark and effective and efficient methods for video individual counting and tracking in large-scale scenes with dense crowds captured by moving drones. We first construct a large-scale video dataset, MovingDroneCrowd++, collected by moving drones in crowded scenes under various shooting angles, flight altitudes, and lighting conditions. Its complex and diverse acquisition conditions make it highly challenging, and existing video individual counting and tracking methods fail to achieve satisfactory performance. To address these challenges, we propose a novel VIC method GD^{3}A and a multi-object tracking method DVTrack, both guided by robust group-wise association based on pixel-level pedestrian descriptor matching which is implemented through OT with the adaptive dustbin score. Based on the group-wise association results, GD^{3}A decomposes the global density map into shared and inflow/outflow density maps, while DVTrack achieves instance-level tracking through a descriptor voting mechanism. Compared with previous methods, our approach achieves substantial performance gains in drone-view scenarios with dense crowds and complex camera motion, reducing the counting error by 47.4% and improving tracking performance by 64.6%. These results demonstrate that our dataset and methods further bridge the gap between theoretical research and practical applications.

References

[1] Y. Jiang, X. Li, G. Zhu, H. Li, J. Deng, K. Han, C. Shen, Q. Shi, and R. Zhang, "Integrated sensing and communication for low altitude economy: Opportunities and challenges," *IEEE Communications Magazine*, pp. 1–7, 2025.

[2] Y. Zhou, "Unmanned aerial vehicles based low-altitude economy with lifecycle techno-economic-environmental analysis for sustainable and smart cities," *Journal of Cleaner Production*, vol. 499, p. 145050, 2025.

[3] V. Lempitsky and A. Zisserman, "Learning to count objects in images," in *Advances in Neural Information Processing Systems*, vol. 23. Curran Associates, Inc., 2010.

[4] Y. Li, X. Zhang, and D. Chen, "Csrnet: Dilated convolutional neural networks for understanding the highly congested scenes," in *Proceedings of the IEEE Conference on Computer Vision and Pattern Recognition (CVPR)*, June 2018.

[5] Q. Song, C. Wang, Z. Jiang, Y. Wang, Y. Tai, C. Wang, J. Li, F. Huang, and Y. Wu, "Rethinking counting and localization in crowds: A purely point-based framework," in *Proceedings of the IEEE/CVF International Conference on Computer Vision (ICCV)*, October 2021, pp. 3365–3374.

[6] Q. Wang, J. Gao, W. Lin, and Y. Yuan, "Learning from synthetic data for crowd counting in the wild," in *Proceedings of the IEEE/CVF Conference on Computer Vision and Pattern Recognition (CVPR)*, June 2019.

[7] R. Gao, J. Qi, and L. Wang, "Multiple object tracking as id prediction," in *Proceedings of the IEEE/CVF Conference on Computer Vision and Pattern Recognition (CVPR)*, June 2025, pp. 27 883–27 893.

[8] D. He, S. Chan, and M. Guizani, "Drone-assisted public safety networks: The security aspect," *IEEE Communications Magazine*, vol. 55, no. 8, pp. 218–223, 2017.

[9] Q. Wang, J. Gao, W. Lin, and X. Li, "Nwpu-crowd: A large-scale benchmark for crowd counting and localization," *IEEE Transactions on Pattern Analysis and Machine Intelligence*, 2020.

[10] H. Idrees, M. Tayyab, K. Athrey, D. Zhang, S. Al-Maadeed, N. Rajpoot, and M. Shah, "Composition loss for counting, density map estimation and localization in dense crowds," in *Proceedings of the European conference on computer vision (ECCV)*, 2018, pp. 532–546.

[11] Y. Zhang, D. Zhou, S. Chen, S. Gao, and Y. Ma, "Single-image crowd counting via multi-column convolutional neural network," in *Proceedings of the IEEE Conference on Computer Vision and Pattern Recognition (CVPR)*, June 2016.

[12] H. Idrees, I. Saleemi, C. Seibert, and M. Shah, "Multi-source multi-scale counting in extremely dense crowd images," in *Proceedings of the IEEE Conference on Computer Vision and Pattern Recognition (CVPR)*, June 2013.

[13] V. A. Sindagi, R. Yasarla, and V. M. Patel, "Jhu-crowd++: Large-scale crowd counting dataset and a benchmark method," *IEEE Transactions on Pattern Analysis and Machine Intelligence*, vol. 44, no. 5, pp. 2594–2609, 2022.

[14] H. Li, L. Liu, K. Yang, S. Liu, J. Gao, B. Zhao, R. Zhang, and J. Hou, "Video crowd localization with multifocus gaussian neighborhood attention and a large-scale benchmark," *IEEE Transactions on Image Processing*, vol. 31, pp. 6032–6047, 2022.

[15] P. Sun, J. Cao, Y. Jiang, Z. Yuan, S. Bai, K. Kitani, and P. Luo, "Dancetrack: Multi-object tracking in uniform appearance and diverse motion," in *Proceedings of the IEEE/CVF Conference on Computer Vision and Pattern Recognition (CVPR)*, June 2022, pp. 20 993–21 002.

[16] P. Dendorfer, H. Rezatofighi, A. Milan, J. Shi, D. Cremers, I. Reid, S. Roth, K. Schindler, and L. Leal-Taixé, "Mot20: A benchmark for multi object tracking in crowded scenes," *arXiv preprint arXiv:2003.09003*, 2020.

[17] Y. Cui, C. Zeng, X. Zhao, Y. Yang, G. Wu, and L. Wang, "Sportsmot: A large multi-object tracking dataset in multiple sports scenes," in *Proceedings of the IEEE/CVF International Conference on Computer Vision (ICCV)*, October 2023, pp. 9921–9931.

[18] H. Lu, X. Zhu, W. Zhang, Y. Li, and X. Bai, "Crowded video individual counting informed by social grouping and spatial-temporal displacement priors," *arXiv preprint arXiv:2601.01192*, 2026.

[19] L. Wen, D. Du, P. Zhu, Q. Hu, Q. Wang, L. Bo, and S. Lyu, "Detection, tracking, and counting meets drones in crowds: A benchmark," in *Proceedings of the IEEE/CVF Conference on Computer Vision and Pattern Recognition (CVPR)*, June 2021, pp. 7812–7821.

[20] Z. Liu, Z. He, L. Wang, W. Wang, Y. Yuan, D. Zhang, J. Zhang, P. Zhu, L. V. Gool, J. Han, S. Hoi, Q. Hu, M. Liu, J. Pan, B. Yin, B. Zhang, C. Liu, D. Ding, D. Liang, G. Ding, H. Lu, H. Lin, J. Chen, J. Li, L. Liu, L. Zhou, M. Shi, Q. Yang, Q. He, S. Peng, W. Xu, W. Han, X. Bai, X. Chen, Y. Wang, Y. Xia, Y. Tao, Z. Chen, and Z. Cao, "Visdrone-cc2021: The vision meets drone crowd counting challenge results," in *2021 IEEE/CVF International Conference on Computer Vision Workshops (ICCVW)*, 2021, pp. 2830–2838.

[21] X. Liu, G. Li, Y. Qi, Z. Yan, Z. Han, A. van den Hengel, M.-H. Yang, and Q. Huang, "Weakly supervised video individual counting," in *Proceedings of the IEEE/CVF Conference on Computer Vision and Pattern Recognition (CVPR)*, June 2024, pp. 19 228–19 237.

[22] P. Zhu, L. Wen, D. Du, X. Bian, H. Fan, Q. Hu, and H. Ling, "Detection and tracking meet drones challenge," *IEEE Transactions on Pattern Analysis and Machine Intelligence*, vol. 44, no. 11, pp. 7380–7399, 2021.

[23] Y. Zhang, P. Sun, Y. Jiang, D. Yu, F. Weng, Z. Yuan, P. Luo, W. Liu, and X. Wang, "Bytetrack: Multi-object tracking by associating every detection box," in *Computer Vision – ECCV 2022*, 2022, pp. 1–21.

[24] T. Meinhardt, A. Kirillov, L. Leal-Taixé, and C. Feichtenhofer, "Trackformer: Multi-object tracking with transformers," in *Proceedings of the IEEE/CVF Conference on Computer Vision and Pattern Recognition (CVPR)*, June 2022, pp. 8844–8854.

[25] Z. Liu, X. Wang, C. Wang, W. Liu, and X. Bai, "Sparsetrack: Multi-object tracking by performing scene decomposition based on pseudo-depth," *IEEE Transactions on Circuits and Systems for Video Technology*, vol. 35, no. 5, pp. 4870–4882, 2025.

[26] R. Luo, Z. Song, L. Ma, J. Wei, W. Yang, and M. Yang, "Diffusiontrack: Diffusion model for multi-object tracking," *Proceedings of the AAAI Conference on Artificial Intelligence*, vol. 38, no. 5, pp. 3991–3999, 2024.

[27] T. Han, L. Bai, J. Gao, Q. Wang, and W. Ouyang, "Dr.vic: Decomposition and reasoning for video individual counting," in *Proceedings of the IEEE/CVF Conference on Computer Vision and Pattern Recognition (CVPR)*, June 2022, pp. 3083–3092.

[28] R. Li, Y. Liu, H. Li, J. Li, and G. Lu, "Prototype-guided dual-transformer reasoning for video individual counting," in *Proceedings of the 32nd ACM International Conference on Multimedia*, 2024, p. 10258–10267.

[29] Y. Fan, J. Wan, T. Han, A. B. Chan, and A. J. Ma, "Video individual counting for moving drones," in *Proceedings of the IEEE/CVF International Conference on Computer Vision (ICCV)*, October 2025, pp. 12 284–12 293.

[30] C.-L. Wan, F.-K. Huang, and H.-H. Shuai, "Density-based flow mask integration via deformable convolution for video people flux estimation," in *Proceedings of the IEEE/CVF Winter Conference on Applications of Computer Vision (WACV)*, January 2024, pp. 6573–6582.

[31] F.-K. Huang, B.-L. Huang, L.-W. Tsao, J.-C. Wu, H.-H. Shuai, and W.-H. Cheng, "Flowing crowd to count flows: A self-supervised framework for video individual counting," ser. MM '25. Association for Computing Machinery, 2025, p. 8234–8243.

[32] G. Peyré, M. Cuturi *et al.*, "Computational optimal transport: With applications to data science," *Foundations and Trends® in Machine Learning*, vol. 11, no. 5-6, pp. 355–607, 2019.

[33] W. Liu, M. Salzmann, and P. Fua, "Context-aware crowd counting," in *Proceedings of the IEEE/CVF Conference on Computer Vision and Pattern Recognition (CVPR)*, June 2019.

[34] Y. Yang, G. Li, Z. Wu, L. Su, Q. Huang, and N. Sebe, "Reverse perspective network for perspective-aware object counting," in *Proceedings of the IEEE/CVF Conference on Computer Vision and Pattern Recognition (CVPR)*, June 2020.

[35] B. Wang, H. Liu, D. Samaras, and M. Hoai, "Distribution matching for crowd counting," in *Advances in Neural Information Processing Systems*, 2020.

[36] T. Han, L. Bai, L. Liu, and W. Ouyang, "Steerer: Resolving scale variations for counting and localization via selective inheritance learning," in *Proceedings of the IEEE/CVF International Conference on Computer Vision (ICCV)*, October 2023, pp. 21 848–21 859.

[37] Y. Ranasinghe, N. G. Nair, W. G. C. Bandara, and V. M. Patel, "Crowddiff: Multi-hypothesis crowd density estimation using diffusion models," in *CVPR*, 2024, pp. 12 809–12 819.

[38] S. An, W. Liu, and S. Venkatesh, "Face recognition using kernel ridge regression," in *2007 IEEE Conference on Computer Vision and Pattern Recognition*, 2007, pp. 1–7.

[39] A. B. Chan, Z.-S. J. Liang, and N. Vasconcelos, "Privacy preserving crowd monitoring: Counting people without people models or tracking," in *2008 IEEE Conference on Computer Vision and Pattern Recognition*, 2008, pp. 1–7.

[40] Z. Yan, Y. Yuan, W. Zuo, X. Tan, Y. Wang, S. Wen, and E. Ding, "Perspective-guided convolution networks for crowd counting," in *Proceedings of the IEEE/CVF International Conference on Computer Vision (ICCV)*, October 2019.

[41] Z. Du, M. Shi, J. Deng, and S. Zafeiriou, "Redesigning multi-scale neural network for crowd counting," *IEEE Transactions on Image Processing*, vol. 32, pp. 3664–3678, 2023.

[42] J. Gao, T. Han, Y. Yuan, and Q. Wang, "Domain-adaptive crowd counting via high-quality image translation and density reconstruction," *IEEE Transactions on Neural Networks and Learning Systems*, vol. 34, no. 8, pp. 4803–4815, 2023.

[43] Z. Du, J. Deng, and M. Shi, "Domain-general crowd counting in unseen scenarios," *Proceedings of the AAAI Conference on Artificial Intelligence*, vol. 37, no. 1, pp. 561–570, Jun. 2023.

[44] H. Xie, Z. Yang, H. Zhu, and Z. Wang, "Striking a balance: Unsupervised cross-domain crowd counting via knowledge diffusion," in *Proceedings of the 31st ACM International Conference on Multimedia*, 2023, p. 6520–6529.

[45] J. Wan, Z. Liu, and A. B. Chan, "A generalized loss function for crowd counting and localization," in *Proceedings of the IEEE/CVF Conference on Computer Vision and Pattern Recognition*, 2021, pp. 1974–1983.

[46] A. B. Chan and N. Vasconcelos, "Bayesian poisson regression for crowd counting," in *2009 IEEE 12th International Conference on Computer Vision*, 2009, pp. 545–551.

[47] D. Liang, W. Xu, and X. Bai, "An end-to-end transformer model for crowd localization," in *Proceedings of the European Conference on Computer Vision (ECCV)*, 2022, pp. 38–54.

[48] Y. Fan, J. Wan, and A. J. Ma, "Learning crowd scale and distribution for weakly supervised crowd counting and localization," *IEEE Transactions on Circuits and Systems for Video Technology*, vol. 35, no. 1, pp. 713–727, 2025.

[49] J. Wan and A. Chan, "Modeling noisy annotations for crowd counting," *Advances in Neural Information Processing Systems*, vol. 33, pp. 3386–3396, 2020.

[50] J. Wan, Q. Wang, and A. B. Chan, "Kernel-based density map generation for dense object counting," *IEEE Transactions on Pattern Analysis and Machine Intelligence*, vol. 44, no. 3, pp. 1357–1370, 2022.

[51] J. Wan and A. Chan, "Adaptive density map generation for crowd counting," in *Proceedings of the IEEE/CVF International Conference on Computer Vision (ICCV)*, October 2019.

[52] H. Mo, X. Zhang, J. Tan, C. Yang, Q. Gu, B. Hang, and W. Ren, "Countformer: Multi-view crowd counting transformer," in *Computer Vision – ECCV 2024*, A. Leonardis, E. Ricci, S. Roth, O. Russakovsky, T. Sattler, and G. Varol, Eds., 2025, pp. 20–40.

[53] Q. Zhang, D. Chen, Y. Gong, and H. Huang, "Synmvcrowd: A large synthetic benchmark for multi-view crowd counting and localization," *International Journal of Computer Vision*, vol. 134, no. 4, p. 191, 2026.

[54] R. Long, Y. Wang, J. Wan, X. Deng, X. Zhu, W. Guan, A. Chan, and L. Nie, "Embodied crowd counting," in *Advances in Neural Information Processing Systems*, D. Belgrave, C. Zhang, H. Lin, R. Pascanu, P. Koniusz, M. Ghassemi, and N. Chen, Eds., vol. 38. Curran Associates, Inc., 2025, pp. 73 692–73 717.

[55] S. Chen, E. Yu, J. Li, and W. Tao, "Delving into the trajectory long-tail distribution for muti-object tracking," in *Proceedings of the IEEE/CVF Conference on Computer Vision and Pattern Recognition (CVPR)*, June 2024, pp. 19 341–19 351.

[56] C. Huang, S. Han, M. He, W. Zheng, and Y. Wei, "Deconfusetrack: Dealing with confusion for multi-object tracking," in *Proceedings of the IEEE/CVF Conference on Computer Vision and Pattern Recognition (CVPR)*, June 2024, pp. 19 290–19 299.

[57] S. You, H. Yao, B.-K. Bao, and C. Xu, "Utm: A unified multiple object tracking model with identity-aware feature enhancement," in *Proceedings of the IEEE/CVF Conference on Computer Vision and Pattern Recognition (CVPR)*, June 2023, pp. 21 876–21 886.

[58] N. Aharon, R. Orfaig, and B.-Z. Bobrovsky, "Bot-sort: Robust associations multi-pedestrian tracking," *arXiv preprint arXiv:2206.14651*, 2022.

[59] W. Lv, Y. Huang, N. Zhang, R.-S. Lin, M. Han, and D. Zeng, "Diffmot: A real-time diffusion-based multiple object tracker with non-linear prediction," in *Proceedings of the IEEE/CVF Conference on Computer Vision and Pattern Recognition (CVPR)*, June 2024, pp. 19 321–19 330.

[60] J. Cao, J. Pang, X. Weng, R. Khirodkar, and K. Kitani, "Observation-centric sort: Rethinking sort for robust multi-object tracking," in *Proceedings of the IEEE/CVF Conference on Computer Vision and Pattern Recognition*, 2023, pp. 9686–9696.

[61] R. E. Kalman, "A new approach to linear filtering and prediction problems," *Journal of Basic Engineering*, vol. 82, no. 1, pp. 35–45, 03 1960.

[62] F. Zeng, B. Dong, Y. Zhang, T. Wang, X. Zhang, and Y. Wei, "Motr: End-to-end multiple-object tracking with transformer," in *Computer Vision – ECCV 2022*, 2022, pp. 659–675.

[63] T. Peng, Q. Li, and P. Zhu, "Rgb-t crowd counting from drone: A benchmark and mmccn network," in *Computer Vision – ACCV 2020*, 2021, pp. 497–513.

[64] L. Wen, D. Du, P. Zhu, Q. Hu, Q. Wang, L. Bo, and S. Lyu, "Drone-based joint density map estimation, localization and tracking with space-time multi-scale attention network," *arXiv preprint arXiv:1912.01811*, 2019.

[65] X. Wang, T. Li, Y. Liu, S. Yao, Y. Liu, N. Yang, and P. Zhu, "A large-scale drone based thermal infrared benchmark and inception transformer network for crowd counting," *Pattern Recognition*, vol. 173, p. 112778, 2026.

[66] M. Zhang, F. Zhao, and Y. Zhang, "Enhanced uav-dot for uav crowd localization: Adaptive gaussian heat map and attention mechanism to address scale/low-light challenges," *Drones*, vol. 9, no. 12, 2025.
[67] M. Alansari, O. A. Hay, S. Alansari, S. Javed, A. Shoufan, Y. Zweiri, and N. Werghi, "Drone-person tracking in uniform appearance crowd: A new dataset," *Scientific Data*, vol. 11, no. 1, p. 15, 2024.
[68] Y. Lei, H. Zhu, J. Yuan, G. Xiang, X. Zhong, and S. He, "Dense-track: Drone-based crowd tracking via density-aware motion-appearance synergy," in *Proceedings of the 32nd ACM International Conference on Multimedia*. Association for Computing Machinery, 2024, p. 2050–2058.
[69] T. Asanomi, K. Nishimura, and R. Bise, "Multi-frame attention with feature-level warping for drone crowd tracking," in *Proceedings of the IEEE/CVF Winter Conference on Applications of Computer Vision (WACV)*, 2023, pp. 1664–1673.
[70] R. Sundararaman, C. De Almeida Braga, E. Marchand, and J. Pettre, "Tracking pedestrian heads in dense crowd," in *Proceedings of the IEEE/CVF Conference on Computer Vision and Pattern Recognition (CVPR)*, June 2021, pp. 3865–3875.
[71] P.-E. Sarlin, D. DeTone, T. Malisiewicz, and A. Rabinovich, "Superglue: Learning feature matching with graph neural networks," in *Proceedings of the IEEE/CVF Conference on Computer Vision and Pattern Recognition (CVPR)*, June 2020.
[72] M. Cuturi, "Sinkhorn distances: Lightspeed computation of optimal transport," in *Advances in Neural Information Processing Systems*, vol. 26, 2013.
[73] J. Munkres, "Algorithms for the assignment and transportation problems," *Journal of the Society for Industrial and Applied Mathematics*, vol. 5, no. 1, pp. 32–38, 1957.
[74] J. Luiten, A. Ošep, P. Dendorfer, P. Torr, A. Geiger, L. Leal-Taixé, and B. Leibe, "Hota: A higher order metric for evaluating multi-object tracking," *International Journal of Computer Vision*, vol. 129, no. 2, pp. 548–578, 2021.
[75] K. Bernardin and R. Stiefelhagen, "Evaluating multiple object tracking performance: the clear mot metrics," *EURASIP Journal on Image and Video Processing*, vol. 2008, no. 1, p. 246309, 2008.
[76] E. Ristani, F. Solera, R. Zou, R. Cucchiara, and C. Tomasi, "Performance measures and a data set for multi-target, multi-camera tracking," in *Computer Vision – ECCV 2016 Workshops*, G. Hua and H. Jégou, Eds. Cham: Springer International Publishing, 2016, pp. 17–35.
[77] K. He, X. Zhang, S. Ren, and J. Sun, "Deep residual learning for image recognition," in *Proceedings of the IEEE Conference on Computer Vision and Pattern Recognition (CVPR)*, June 2016.
[78] T.-Y. Lin, P. Dollar, R. Girshick, K. He, B. Hariharan, and S. Belongie, "Feature pyramid networks for object detection," in *Proceedings of the IEEE Conference on Computer Vision and Pattern Recognition (CVPR)*, July 2017.
[79] Z. Zhao, H. Li, R. Zhao, and X. Wang, "Crossing-line crowd counting with two-phase deep neural networks," in *Computer Vision – ECCV 2016*, 2016, pp. 712–726.
[80] Y. Zhang, C. Wang, X. Wang, W. Zeng, and W. Liu, "Fairmot: On the fairness of detection and re-identification in multiple object tracking," *International Journal of Computer Vision*, vol. 129, no. 11, pp. 3069–3087, 2021.
[81] X. Zhu, J. Xu, B. Wang, H. Dai, and H. Lu, "Video individual counting with implicit one-to-many matching," in *2025 IEEE International Conference on Image Processing (ICIP)*, 2025, pp. 61–66.